

## Identification, Characterization and Initial Hit-to-Lead Optimization of a Series of 4-Arylamino-3-Pyridinecarbonitrile as Protein Kinase C theta (PKC $\theta$ ) Inhibitors

Derek C. Cole,\*<sup>†</sup> Magda Asselin,<sup>†</sup> Agnes Brennan,<sup>‡</sup> Robert Czerwinski,<sup>§</sup> John W. Ellingboe,<sup>†</sup> Lori Fitz,<sup>‡</sup> Rita Greco,<sup>‡</sup> Xinyi Huang,<sup>||</sup> Diane Joseph-McCarthy,<sup>+§</sup> Michael F. Kelly,<sup>†</sup> Matthew Kirisits,<sup>†</sup> Julie Lee,<sup>‡</sup> Yuanhong Li,<sup>§</sup> Paul Morgan,<sup>‡</sup> Joseph R. Stock,<sup>†</sup> Désirée H. H. Tsao,<sup>§</sup> Allan Wissner,<sup>†</sup> Xiaoke Yang,<sup>‡</sup> and Divya Chaudhary<sup>‡</sup>

Chemical and Screening Sciences, Wyeth Research, 401 North Middletown Road, Pearl River, New York 10965, Inflammation and Chemical and Screening Sciences, Wyeth Research, 200 Cambridge Park Drive, Cambridge, Massachusetts 02140, Chemical and Screening Sciences, Wyeth Research, 500 Arcola Road, Collegeville, Pennsylvania 19426

Received February 28, 2008

The protein kinase C (PKC) family of serine/threonine kinases is implicated in a wide variety of cellular processes. The PKC theta (PKC $\theta$ ) isoform is involved in TCR signal transduction and T cell activation and regulates T cell mediated diseases, including lung inflammation and airway hyperresponsiveness. Thus inhibition of PKC $\theta$  enzyme activity by a small molecule represents an attractive strategy for the treatment of asthma. A PKC $\theta$  high-throughput screening (HTS) campaign led to the identification of 4-(3-bromophenylamino)-5-(3,4-dimethoxyphenyl)-3-pyridinecarbonitrile **4a**, a low  $\mu$ M ATP competitive PKC $\theta$  inhibitor. Structure based hit-to-lead optimization led to the identification of 5-(3,4-dimethoxyphenyl)-4-(1*H*-indol-5-ylamino)-3-pyridinecarbonitrile **4p**, a 70 nM PKC $\theta$  inhibitor. Compound **4p** was selective for inhibition of novel PKC isoforms over a panel of 21 serine/threonine, tyrosine, and phosphoinositol kinases, in addition to the conventional and atypical PKCs, PKC $\beta$ , and PKC $\zeta$ , respectively. Compound **4p** also inhibited IL-2 production in antiCD3/anti-CD28 activated T cells enriched from splenocytes.

### Introduction

The protein kinase C (PKC)<sup>a</sup> family of serine/threonine kinases consists of 11 isoforms that share sequence and structural homology but vary in their activation, tissue expression, and cellular regulation.<sup>1</sup> PKCs have been implicated in a wide variety of cellular processes, including growth, differentiation, secretion, apoptosis, and tumor development.<sup>2</sup> These kinases are classified based on their cofactor requirements: conventional (cPKCs:  $\alpha$ ,  $\beta$ ,  $\gamma$ ) require both Ca<sup>2+</sup> and diacylglycerol (DAG) as cofactors, novel (nPKCs:  $\delta$ ,  $\epsilon$ ,  $\theta$ ,  $\eta$ ) require DAG but are Ca<sup>2+</sup> independent and atypical (aPKCs:  $\iota$ ,  $\lambda$ ,  $\zeta$ ) do not require Ca<sup>2+</sup> or DAG.<sup>3</sup>

The nPKC, PKC theta (PKC $\theta$ ) was first characterized in 1993 and displays the highest homology PKC $\delta$ . PKC $\theta$  transcripts are expressed in several cell types, with predominant expression in T cells and thymocytes.<sup>4</sup> PKC $\theta$  transduces the T cell receptor (TCR) stimulation signal to the activation of transcription factors, inducing interleukin-2 (IL-2) expression and T cell

activation.<sup>5,6</sup> PKC $\theta$  signaling regulates lung inflammation and airway hyperresponsiveness in mouse models of antigen induced asthma.<sup>7,8</sup> In models of experimental autoimmune encephalomyelitis (EAE), PKC $\theta$  deficient mice have reduced T cell and macrophage infiltration and demyelination in the brain compared with wild-type control mice in response to antigen challenge.<sup>9,10</sup> In addition PKC $\theta$  deficient mice also have a significantly diminished response in the type II collagen-induced arthritis (CIA) model, however mount normal protective Th1 immune responses to clear virus infection.<sup>11,12</sup>

Therefore PKC $\theta$  is a critical enzyme that regulates selective T cell function and represents an attractive drug target for asthma<sup>8</sup> and other T cell-mediated diseases,<sup>13</sup> such as multiple sclerosis<sup>9,10</sup> and arthritis.<sup>12</sup> The sequential ordered catalytic mechanism<sup>14</sup> and the structure of phosphorylated human recombinant PKC $\theta$  kinase domain (KD) cocrystallized with staurosporine<sup>15</sup> have been reported, and these findings may aid inhibitor optimization. Of importance is selectivity over the closely related PKC $\delta$  since this kinase negatively regulates B cell proliferation in mice.<sup>2,16</sup>

Several classes of inhibitors that bind to the C1 domains of PKCs have been described, including the diterpenes such as phorbol esters,<sup>17–19</sup> macrocyclic lactones such as bryostatins,<sup>19,20</sup> polyacetates such as aplysiatoxin, indole alkaloids such as teleocidin,<sup>21</sup> and diacylglycerol analogues.<sup>22,23</sup> Several bisindolemaleimide or staurosporine analogues including *N*-benzoyl-staurosporine (midostaurin),<sup>24</sup> 7-hydroxystaurosporine (UCN01)<sup>25,26</sup> and (9*S*)-9-[(dimethylamino)methyl]-6,7,10,11-tetrahydro-9*H*, 18*H*-5,21:12,17-dimethenodibenzo[*e,k*]pyrrolo[3,4-*h*][1,4,13]-oxadiazacyclohexadecine-18,20(19*H*)-dione (ruboxistaurin, LY-335351)<sup>27,28</sup> with varying degrees of selectivity for cPKCs have entered clinical trials for oncology and diabetes related complications.<sup>29</sup> Recently 2,4-diaminopyrimidines have been reported as PKC $\theta$  inhibitors.<sup>30</sup>

Here we report the identification of a novel series of 4-arylamino-3-pyridinecarbonitriles as selective nPKC, and in

\* To whom correspondence should be addressed. Phone: 845 602-4619. Fax: 845 602-5561. E-mail: coledc@wyeth.com.

<sup>†</sup> Chemical and Screening Sciences, Wyeth Research, Pearl River, New York.

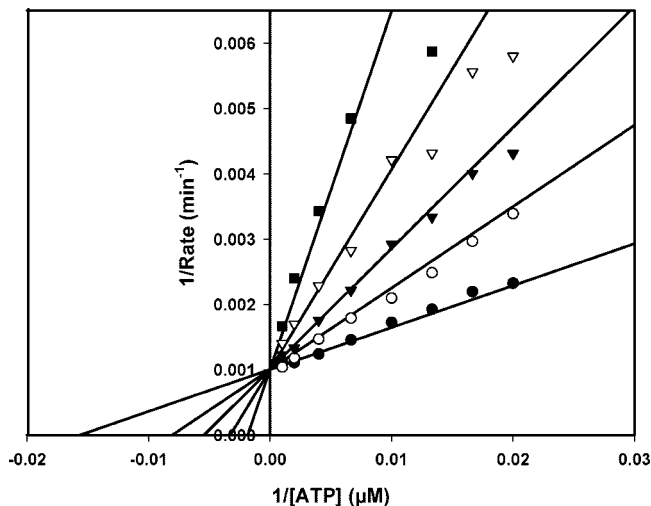
<sup>‡</sup> Inflammation Sciences, Wyeth Research, Cambridge, Massachusetts.

<sup>§</sup> Chemical and Screening Sciences, Wyeth Research, Cambridge Massachusetts.

<sup>||</sup> Chemical and Screening Sciences, Wyeth Research, Collegeville, Pennsylvania.

<sup>+</sup> Current address: AstraZeneca, Waltham, Massachusetts 02451.

<sup>a</sup> Abbreviations: PKC, protein kinase C; PKC $\alpha$ , protein kinase C alpha; PKC $\beta$ , protein kinase C beta; PKC $\gamma$ , protein kinase C gamma; PKC $\delta$ , protein kinase C delta; PKC $\epsilon$ , protein kinase C epsilon; PKC $\theta$ , protein kinase C theta; PKC $\eta$ , protein kinase C eta; PKC $\lambda$ , protein kinase C iota; PKC $\lambda$ , protein kinase C lambda; PKC $\zeta$ , protein kinase C zeta; HTS, high-throughput screen; DAG, diacylglycerol; TCR, T cell receptor; EAE, experimental autoimmune encephalomyelitis; CIA, collagen-induced arthritis; KD, kinase domain; IL-2, interleukin-2; FITC, fluorescein isothiocyanate; BIM-I, bisindolemaleimide I; FP, fluorescent polarization; FITC-BIM-I, fluorescein isothiocyanate-BIM-I; STD, saturation transfer difference; IMAP, kinase assay from Molecular Devices.



**Figure 1.** Lineweaver–Burk plot for inhibition of PKC $\theta$  by **4a**. Inhibitor concentration: 0.0 (●), 3.75 (○), 7.5 (▼), 15.0 (▽) and 30.0  $\mu$ M (■).  $K_i = 4.9 \pm 0.3$ .

particular PKC $\theta$  inhibitors. Biophysical characterization experiments were used to confirm an ATP competitive mode of inhibition of the active PKC $\theta$  catalytic kinase domain (KD). Hit-to-lead optimization led to the identification of **4p** as an attractive small molecule lead (MW = 370, clogP = 4.4) with low nM PKC $\theta$  inhibitory activity, selectivity over several other kinases, and good cellular activity in the inhibition of T cell IL-2 production.

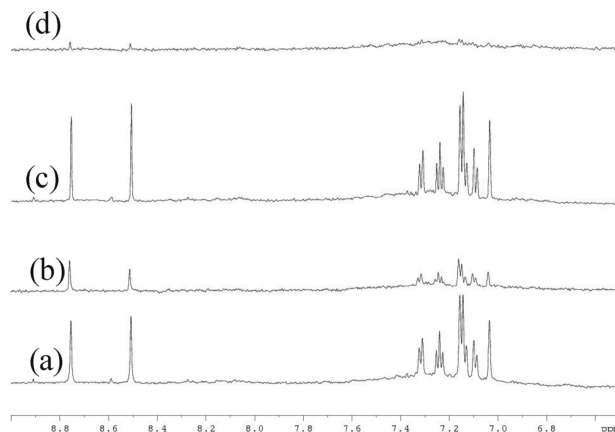
## Results and Discussion

High-throughput screening (HTS) of Wyeth's corporate compound collection using a Caliper based assay<sup>31</sup> with purified recombinant active PKC $\theta$  (KD) (amino acids 362–706)<sup>14</sup> led to the identification of a small molecule inhibitor 4-(3-bromophenylamino)-5-(3,4-dimethoxy-phenyl)-3-pyridinecarbonitrile **4a** with low  $\mu$ M enzyme inhibition activity. Binding experiments show **4a** binds competitively with ATP with a  $K_i$  of 4.9  $\mu$ M (Figure 1).

Fluorescence polarization (FP) competition displacement experiments<sup>32</sup> were carried out using a fluorescent probe (FITC-BIM-I; IC<sub>50</sub> = 150 nM) prepared by coupling fluorescein isothiocyanate (FITC) and an analogue of bisindolemaleimide I (BIM-I)<sup>33</sup> a known potent ATP competitive PKC $\theta$  inhibitor. Preliminary results show the HTS hit **4a** partially displaced the fluorescent probe binding to PKC $\theta$  (data not shown), consistent with an ATP site interaction. The FP competition displacement experiment was complicated by interactions observed between the probe and **4a** in the absence of PKC $\theta$ .

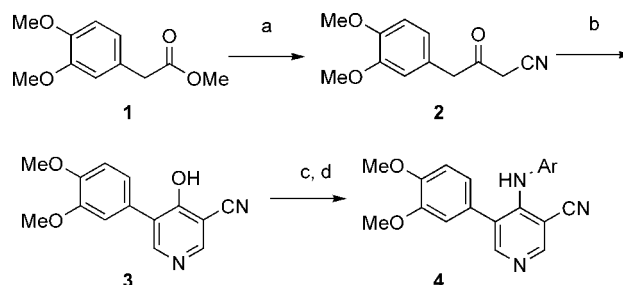
Hit characterization using NMR binding studies performed by saturation transfer difference (STD)<sup>34</sup> experiment showed a strong STD signal for **4a**, with PKC $\theta$  indicating binding of **4a** to the protein (Figure 2b). The interaction signal is almost completely eliminated by the addition of BIM-I (Figure 2d), indicating displacement by the more potent BIM-I, further suggesting that the two inhibitors compete for the ATP binding pocket.

An initial array of compounds was prepared to explore the SAR of the headpiece aryl group following the route in Scheme 1. 3,4-Dimethoxyphenyl acetic acid methyl ester **1** was reacted with the lithium anion of acetonitrile to give 4-(3,4-dimethoxyphenyl)-3-oxo-butyro-nitrile **2** in 75% overall yield. Reaction with DMF-DMA in DMF at 122 °C overnight followed by reaction with ammonium acetate in refluxing ethanol gave the

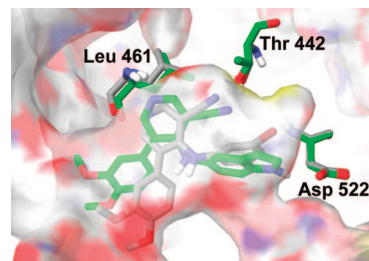


**Figure 2.** (A and B) <sup>1</sup>H NMR spectra of **4a** (80  $\mu$ M) and PKC $\theta$  (3  $\mu$ M). (A) <sup>1</sup>H NMR spectrum; (B) saturation transfer difference (STD) spectrum, showing that **4a** binds to PKC $\theta$ . (C and D) <sup>1</sup>H NMR spectrum of **4a** and PKC $\theta$  with addition of BIM-I (5  $\mu$ M). (C) <sup>1</sup>H NMR spectrum; (D) STD spectrum, showing reduction of **4a** STD peaks due to competition by BIM-I.

## Scheme 1<sup>a</sup>



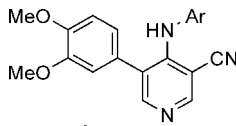
<sup>a</sup> (a) ACN, n-BuLi, -78°C, THF. (b) (i) DMF-DMA, 122°C, 16 h, DMF; (ii) NH<sub>4</sub>OAc, EtOH 85°C, 1 h. (c) POCl<sub>3</sub> 125°C, 1.5 h. (d) ArNH<sub>2</sub>, Pyr·HCl, 135°C, 8 h, EtOEtOH.



**Figure 3.** Model of **4a** (carbon atoms in gray) and **4p** (carbon atoms in green) bound to the ATP site of PKC $\theta$ .

5-(3,4-dimethoxyphenyl)-4-hydroxy-3-pyridinecarbonitrile **3** in 69% yield. Reaction in refluxing phosphorus oxychloride gave the corresponding 4-chloro-5-(3,4-dimethoxy-phenyl)-3-pyridinecarbonitrile in 91% yield and displacement of the chloride by a set of anilines by reaction in refluxing 2-ethoxyethanol in the presence of pyridine hydrochloride gave the target compounds **4a–r**, which were assayed for PKC $\theta$  inhibitory activity in a fluorescence polarization kinase assay.<sup>35</sup>

A computational model of **4a** bound to the PKC $\theta$  ATP site based on the staurosporine bound PKC $\theta$  cocrystal structure<sup>15</sup> indicates the molecule is locked in place by a hydrogen bonding interaction between the pyridine nitrogen and the backbone N–H of the hinge region residue Leu<sup>461</sup> (Figure 3). The nitrile functionality forms an additional polar interaction with the side chain of the gatekeeper residue, Thr<sup>442</sup>, and the 3-bromophenyl moiety extends deep into the

**Table 1.** PKC $\theta$  IC<sub>50</sub> Values for **4a–r**


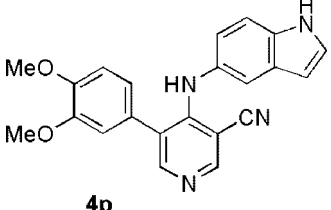
	Ar	PKC $\theta$ IC <sub>50</sub> ( $\mu$ M) <sup>a</sup>
<b>4a</b>	3-bromophenyl	4.6 $\pm$ 1.0
<b>4b</b>	phenyl	1.6 $\pm$ 0.2
<b>4c</b>	3-chlorophenyl	3.9 $\pm$ 1.9
<b>4d</b>	3-fluorophenyl	1.4 $\pm$ 0.5
<b>4e</b>	3-phenoxyphenyl	>30
<b>4f</b>	3-benzyloxyphenyl	>30
<b>4g</b>	4-chlorophenyl	2.8 $\pm$ 0.7
<b>4h</b>	4-methylphenyl	0.9 $\pm$ 0.1
<b>4i</b>	4-methoxyphenyl	0.4 $\pm$ 0.0
<b>4j</b>	4-phenoxyphenyl	8.4 $\pm$ 3.5
<b>4k</b>	2,4-dichlorophenyl	0.08 $\pm$ 0.01
<b>4l</b>	2,4-dimethylphenyl	0.16 $\pm$ 0.01
<b>4m</b>	2,5-dichlorophenyl	0.47 $\pm$ 0.10
<b>4n</b>	3,4-dichlorophenyl	2.4 $\pm$ 0.1
<b>4o</b>	3,4-dimethoxyphenyl	2.2 $\pm$ 0.4
<b>4p</b>	5-indolyl	0.07 $\pm$ 0.03
<b>4q</b>	6-indolyl	2.2 $\pm$ 0.4
<b>4r</b>	5-indanyl	2.0 $\pm$ 0.5

<sup>a</sup> IC<sub>50</sub> values are the average of three determinations in the PKC $\theta$  fluorescence polarization kinase assay (Molecular Devices).

selectivity pocket. The model suggests the bromine atom may be slightly too large, forcing the molecule to shift and somewhat weaken the pyridine nitrogen to hinge the *N–H* hydrogen bond. This is consistent with initial analogues prepared that show the unsubstituted, 3-chloro, and 3-fluoro phenyl analogues (**4b–4d**) have up to 3-fold higher inhibitory activity (Table 1). Other larger substitutions such as phenoxy (**4e**) and benzyloxy (**4f**) are also not tolerated at the 3-position. Moving the halo substitution to the 4-position as in **4g** had little effect on the inhibitory activity. The 4-methyl analogue **4h** was about 3-fold more potent, while the 4-methoxy analogue **4i** was about 6-fold more active (PKC $\theta$  IC<sub>50</sub> = 406 nM). Once again the larger phenoxy group (**4j**) was not tolerated at the 4-position.

A small lipophilic pocket adjacent to the *ortho*-position of the head-piece aryl group was exploited and gave a significant increase in inhibitory activity as shown by the 2,4-dichloro and 2,4-dimethyl analogues (**4k**, **4l**). Similar to the weaker *meta*-substituted analogues (**4a**, **4c**, and **4d**) bis-substituted analogues that included a *meta*-group, e.g., the 2,5-dichloro (**4m**) and the 3,4-disubstituted analogues (**4n** and **4o**) were not well-tolerated and led to weaker inhibitory activity.

The initial model of **4a** suggested that the addition of a hydrogen bond donating group at the 4-position of the headgroup phenyl ring could form an additional hydrogen bonding interaction with the side chain of Asp<sup>522</sup> (the phenyl group 4-position is 3.9 Å from the Asp<sup>522</sup> OD1). The presence of this *N–H* bond acceptor in the region adjacent to the 4-position of the headpiece was targeted by the 5-aminoindolyl analogue **4p**. The model of **4p** bound to PKC $\theta$  (Figure 3, carbons in green) indicates that the indole headpiece *N–H* moiety interacts with Asp<sup>522</sup> and allows the molecule to rotate slightly, potentially increasing the strength of the pyridine nitrogen to hinge *N–H* hydrogen bond. We confirmed the 5-aminoindolyl group potentially facilitating this H-bonding interaction by observing a significant increase in potency. The corresponding 6-indolyl and 5-indanyl analogue **4q** and **4r** were approximately 20-fold less potent, indicating

**Table 2.** Enzyme Inhibition and Binding Data for **4p** against PKC Isoforms


PKC type	isoform	IC <sub>50</sub> ( $\mu$ M) <sup>a</sup>	K <sub>i</sub> ( $\mu$ M) <sup>b</sup>
conventional	$\beta$	>50	
novel	$\delta$	0.35 $\pm$ 0.12	1.6 $\pm$ 0.2
	$\epsilon$	2.33 $\pm$ 1.19	
	$\theta$	0.07 $\pm$ 0.03	0.079 $\pm$ 0.004
	$\eta$	16.35 $\pm$ 1.48	
atypical	$\zeta$	>50	

<sup>a</sup> IC<sub>50</sub> values are the average of three determinations from fluorescence polarization assay (Molecular Devices). <sup>b</sup> K<sub>i</sub> values are the average of three independent determinations.

the activity of **4p** is likely predominantly due to this additional H-bonding interaction and not merely filling space in the protein surface.

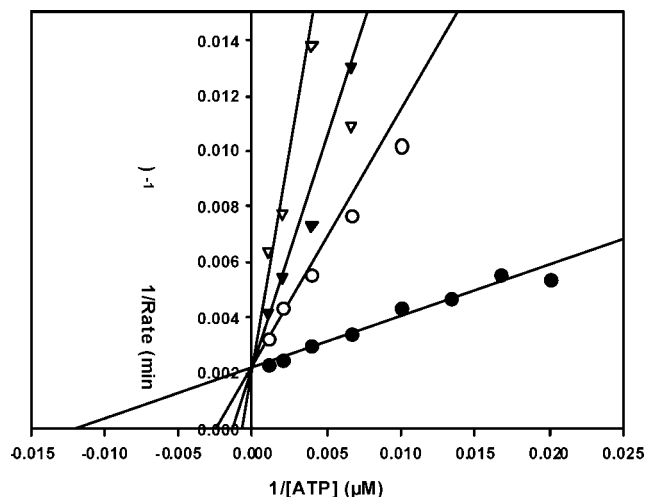
Compound **4p** was found to have good selectivity for PKC $\theta$  inhibition when assayed in a panel of PKC isozyme kinase assays (Table 2). No inhibition was observed for either the conventional PKC isoform PKC $\beta$  or the atypical isoform PKC $\zeta$  at the highest concentration tested (50  $\mu$ M). In the novel family, **4p** had good selectivity against PKC $\epsilon$  and PKC $\eta$ , 33- and >200-fold, respectively, and was 5-fold selective for inhibition of PKC $\theta$  versus the very closely related PKC $\delta$ . Binding experiments showed **4p** binds approximately 20-fold more tightly to PKC $\theta$  than PKC $\delta$ .

Additionally, compound **4p** was selective for the PKC family with an IC<sub>50</sub> of greater than 10  $\mu$ M against a wide variety of kinases including serine/threonine kinases (MK2, Plk, Akt, PKA, Raf, Tpl2, CDK4, p70 S6, IKK, PDK1), tyrosine kinases (Lyn, Src, Lck, BTK, EGFR, IGFR, KDR), and phosphoinositol-3-kinase (PI3K $\alpha$ ).

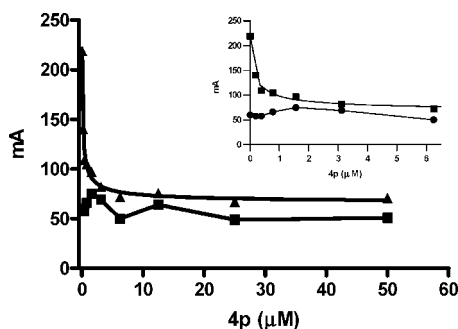
Compound **4p** was found to display kinetics consistent with direct competition for ATP binding to PKC $\theta$ . The ATP concentration was varied in a series of inhibition experiments of PKC $\theta$  kinase assay with **4p**. A Lineweaver–Burk double-reciprocal dose–response plot (Figure 4) of reaction rates against ATP concentration from the inhibition experiments was consistent with **4p** acting as a direct competitive inhibitor with ATP for binding to PKC $\theta$  with an apparent K<sub>i</sub> = 0.079  $\mu$ M, consistent with the observed IC<sub>50</sub> value (PKC $\theta$  IC<sub>50</sub> = 0.07  $\mu$ M).

In contrast to the relatively weaker HTS hit **4a** (PKC $\theta$  IC<sub>50</sub> = 4.6  $\mu$ M) the more potent inhibitor **4p** (PKC $\theta$  IC<sub>50</sub> = 0.07  $\mu$ M) completely displaced the fluorescent probe, consistent with the tighter binding of the inhibitor to the ATP binding site of PKC $\theta$  (Figure 5). The IC<sub>50</sub> from FP displacement (IC<sub>50</sub> = 0.15  $\mu$ M) was also consistent with the K<sub>i</sub> and enzyme inhibition IC<sub>50</sub>.

Having established selectivity in a panel of kinase enzyme assays, **4p** was next evaluated for inhibition of PKC $\theta$  in T cell activation by stimulating splenocyte derived T cells. Compound **4p** was shown to inhibit IL-2 production in anti-CD3 and anti-CD28 activated T cells from normal wild-type and PKC $\theta$  knockout mice with IC<sub>50</sub> values of 0.058 and 0.231  $\mu$ M, respectively (Figure 6). The approximately 4-fold selectivity in comparing T cells deficient in PKC $\theta$ , suggests on-target



**Figure 4.** Lineweaver–Burk plot for inhibition of PKC $\theta$  by **4p**. Inhibitor concentration: 0.0 (●), 0.5 (○), 1.0 (▼), and 2.0 (▽).  $K_i = 0.079 \pm 0.004 \mu\text{M}$ .



**Figure 5.** Fluorescent polarization (FP) competition displacement of FITC-BIM-I ( $IC_{50} = 150 \text{ nM}$ ) by **4p** (▲). In the control reaction, **4p** and the FP probe are incubated in the absence of PKC $\theta$  (■).

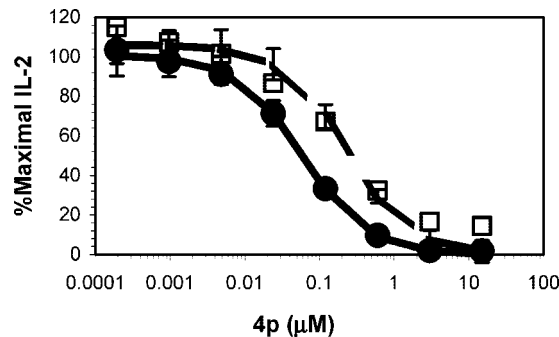
inhibitory activity relative to inhibition of kinases other than PKC $\theta$  which contribute to IL-2 production in the T cell signaling pathway.

## Conclusion

Using a HTS Caliper kinase assay we identified a small lead like inhibitor of PKC $\theta$ . Initial hit-to-lead optimization led to the identification of 5-(3,4-dimethoxyphenyl)-4-(1*H*-indol-5-ylamino)-3-pyridinecarbonitrile **4p**, a 70 nM PKC $\theta$  inhibitor with excellent selectivity over several unrelated kinases, as well as conventional and novel PKCs and modest selectivity over the closely related PKC $\delta$ . Future work will describe the continued optimization and in vivo efficacy studies of this very promising series of PKC $\theta$  inhibitors.

## Experimental Methods

NMR spectra were recorded on a Bruker Avance 300 MHz spectrometer. All chemical shifts are reported in parts per million ( $\delta$ ) relative to tetramethylsilane. The following abbreviations are used to denote signal patterns: s = singlet, d = doublet, t = triplet, m = multiplet and b = broad. The mass spectral data were determined on an Agilent 1100 series LC/MSD and HRMS was carried out on a Bruker APEX II 9.4 T mass spectrometer. Manual silica gel flash chromatography was performed using bulk Silica Gel 60 (230–400 mesh) from EMD Chemicals, Inc. Automated flash chromatography was carried out on a Teledyne Isco, Inc. CombiFlash Companion using RediSep silica gel cartridges. Reverse phase HPLC purifications were performed on a Gilson preparative HPLC system controlled by Unipoint software using either Phe-



**Figure 6.** Inhibition of IL-2 production by **4p**. IL-2 levels from anti-CD3 and anti-CD28 activated T cell-enriched splenocytes from wild-type (●) and PKC $\theta$  knockout (□) mice. Results and error bars represents an average of three independent determinations, each in triplicate.

nomenex Gemini 100 mm  $\times$  21.2 mm or Waters Xterra Prep 5  $\mu\text{M}$ , 100 mm  $\times$  19 mm C $_{18}$  columns and in a 10–90% acetonitrile in water solvent gradient with 0.02% TFA buffer.

**4-(3,4-Dimethoxyphenyl)-3-oxo-butyronitrile (2).** To a 1.0 L three-necked round-bottomed flask was added 50 mL of THF and the reaction mixture was cooled to  $-78 \text{ }^\circ\text{C}$ . Butyl lithium (1.6 M, 14.4 mL, 23 mmol) was added dropwise keeping the temperature below  $-70 \text{ }^\circ\text{C}$ . Acetonitrile (1.3 mL, 25 mmol) in 30 mL of THF was added dropwise to the flask with stirring and cooling. After 2 h of stirring, 3,4-dimethoxyphenyl)acetic acid methyl ester (2.3 g, 11 mmol) was added to the resulting white colloidal mixture in the flask. The reaction mixture was stirred for a further two hours, followed by the addition of saturated ammonium chloride solution (75 mL) at  $-78 \text{ }^\circ\text{C}$ . The organic layer was separated, dried with sodium sulfate, filtered to remove the drying agent, and evaporated to dryness to give the crude product. This crude product was purified by flash chromatography on silica gel eluting with 30–70% ethyl acetate in hexanes to yield a solidifying amber oil, 1.8 g (75%); mp:  $78\text{--}80 \text{ }^\circ\text{C}$ .  $^1\text{H NMR}$  (400 MHz, DMSO- $d_6$ )  $\delta$  6.89 (d,  $J = 8.0 \text{ Hz}$ , 1H), 6.79 (d,  $J = 2.4 \text{ Hz}$ , 1H), 6.70 (dd,  $J = 8.0, 2.4 \text{ Hz}$ , 1H), 4.07 (s, 2H), 3.75 (s, 2H), 3.73 (s, 3H), 3.72 (s, 3H). HRMS  $m/z$  242.07821, calcd  $[\text{M} + \text{Na}]^+$  242.07876, rel int 100%, error  $-0.55 \text{ mAmu}$ . Anal. Calcd for C $_{12}\text{H}_{13}\text{NO}_3$ : C, 65.74; H, 5.98; N, 6.39. Found: C, 65.77; H, 6.25; N, 6.36.

**5-(3,4-Dimethoxyphenyl)-4-hydroxy-3-pyridinecarbonitrile (3).** To a solution of 4-(3,4-dimethoxyphenyl)-3-oxo-butyronitrile (5.0 g, 23 mmol) in DMF (12 mL) was added DMF-DMA (13.5 mL, 101 mmol) and the solution heated at  $122 \text{ }^\circ\text{C}$  overnight. Concentration on a rotovap under high vacuum gave an orange-red solid. This solid was dissolved in EtOH (100 mL), and excess ammonium acetate was added and the reaction mixture was heated at  $85 \text{ }^\circ\text{C}$  for 1 h. The reaction mixture was allowed to cool to r.t. for 1 h, then the solids were collected by filtration and washed with cold EtOH to give a brown solid (4.1 g, 69%); mp:  $>260 \text{ }^\circ\text{C}$ .  $^1\text{H NMR}$  (400 MHz, DMSO- $d_6$ )  $\delta$  12.43 (b, 1H), 8.45 (d,  $J = 1.6 \text{ Hz}$ , 1H), 7.96 (d,  $J = 1.9 \text{ Hz}$ , 1H), 7.28 (d,  $J = 2.0 \text{ Hz}$ , 1H), 7.21 (dd,  $J = 8.2, 2.1 \text{ Hz}$ , 1H), 6.97 (d,  $J = 8.2 \text{ Hz}$ , 1H), 3.77 (s, 3H), 3.76 (s, 3H). HRMS  $m/z$  257.09152, calcd  $[\text{M} + \text{H}]^+$  257.06207, rel int 100%, error  $-0.55 \text{ mAmu}$ .

**4-Chloro-5-(3,4-dimethoxyphenyl)-3-pyridinecarbonitrile.** A solution of 5-(3,4-dimethoxyphenyl)-4-hydroxy-3-pyridinecarbonitrile (4 g, 15.7 mmol) in POCl $_3$  (25 mL) was heated at  $125 \text{ }^\circ\text{C}$  for 90 min, cooled to r.t. and poured into a mixture of ice, 3 N sodium hydroxide, and ethyl acetate. The resulting mixture was stirred and the layers separated. The organic layer was dried over MgSO $_4$ , filtered, and concentrated to give 3.9 g (91% yield) of a brown solid, which was used directly in the next step; mp:  $160\text{--}162 \text{ }^\circ\text{C}$ .  $^1\text{H NMR}$  (400 MHz, DMSO- $d_6$ )  $\delta$  9.07 (s, 1H), 8.87 (s, 1H), 7.15–7.09 (m, 3H), 3.82 (s, 3H), 3.79 (s, 3H). HRMS  $m/z$  275.05871, calcd  $[\text{M} + \text{H}]^+$  275.05819, rel int 4%, error 0.52 mAmu. Anal. Calcd for C $_{14}\text{H}_{11}\text{ClN}_2\text{O}_2$ : C, 61.21; H, 4.04; N, 10.20. Found: C, 61.00; H, 4.34; N, 10.11.

**Table 3.** HPLC Purity and HRMS Data for **4a–r**

compd	A r.t. (min) <sup>a</sup>	A purity (%) <sup>a</sup>	B r.t. (min) <sup>b</sup>	B purity (%) <sup>b</sup>	formula	calcd [M + H] <sup>+</sup>	found [M + H] <sup>+</sup>	rel int	error (mAmu)
<b>4a</b>	2.65	100	2.59	100	C <sub>20</sub> H <sub>16</sub> Br <sub>1</sub> N <sub>3</sub> O <sub>2</sub>	410.04987	410.04987	100	0.01
<b>4b</b>	2.16	97.9	2.43	100	C <sub>20</sub> H <sub>17</sub> N <sub>3</sub> O <sub>2</sub>	332.13936	332.13998	100	0.62
<b>4c</b>	2.06	100	2.59	100	C <sub>20</sub> H <sub>16</sub> Cl <sub>1</sub> N <sub>3</sub> O <sub>2</sub>	366.10038	366.10032	100	-0.06
<b>4d</b>	2.43	100	2.50	100	C <sub>20</sub> H <sub>16</sub> F <sub>1</sub> N <sub>3</sub> O <sub>2</sub>	350.12993	350.13021	100	0.28
<b>4e</b>	2.91	100	2.90	100	C <sub>26</sub> H <sub>21</sub> N <sub>3</sub> O <sub>3</sub>	424.16557	424.16494	100	-0.63
<b>4f</b>	2.91	100	2.93	100	C <sub>27</sub> H <sub>23</sub> N <sub>3</sub> O <sub>3</sub>	438.18122	438.18139	100	0.17
<b>4g</b>	2.55	100	2.73	100	C <sub>20</sub> H <sub>16</sub> Cl <sub>1</sub> N <sub>3</sub> O <sub>2</sub>	366.10038	366.10109	100	0.71
<b>4h</b>	2.29	97.1	2.73	100	C <sub>21</sub> H <sub>19</sub> N <sub>3</sub> O <sub>2</sub>	346.15501	346.15515	100	0.14
<b>4i</b>	2.07	100	2.61	100	C <sub>21</sub> H <sub>19</sub> N <sub>3</sub> O <sub>3</sub>	362.14992	362.15036	100	0.44
<b>4j</b>	2.82	100	3.04	100	C <sub>26</sub> H <sub>21</sub> N <sub>3</sub> O <sub>3</sub>	424.16557	424.16635	100	0.78
<b>4k</b>	2.84	96.3	2.92	100	C <sub>20</sub> H <sub>15</sub> Cl <sub>2</sub> N <sub>3</sub> O <sub>2</sub>	400.06141	400.0612	100	-0.21
<b>4l</b>	2.34	100	2.85	100	C <sub>22</sub> H <sub>21</sub> N <sub>3</sub> O <sub>2</sub>	360.17066	360.17096	100	0.3
<b>4m</b>	2.89	100	2.89	100	C <sub>20</sub> H <sub>15</sub> Cl <sub>2</sub> N <sub>3</sub> O <sub>2</sub>	400.06141	400.06099	100	-0.42
<b>4n</b>	2.89	100	2.99	100	C <sub>20</sub> H <sub>15</sub> Cl <sub>2</sub> N <sub>3</sub> O <sub>2</sub>	400.06141	400.06236	100	0.95
<b>4o</b>	1.97	100	2.92	100	C <sub>22</sub> H <sub>21</sub> N <sub>3</sub> O <sub>4</sub>	392.16049	392.16076	100	0.27
<b>4p</b>	1.96	100	2.71	100	C <sub>22</sub> H <sub>18</sub> N <sub>4</sub> O <sub>2</sub>	371.15026	371.15104	100	0.78
<b>4q</b>	2.09	98.0	2.71	100	C <sub>22</sub> H <sub>18</sub> N <sub>4</sub> O <sub>2</sub>	371.15026	371.15064	100	0.38
<b>4r</b>	2.51	100	3.00	100	C <sub>23</sub> H <sub>21</sub> N <sub>3</sub> O <sub>2</sub>	372.17066	372.17115	100	0.49

<sup>a</sup> HPLC method A: solvent gradient = 90% A @ 0 min, 10% A @ 3.5 min, 10% A @ 5 min; solvent A = 0.1% formic acid in water; solvent B = 0.1% formic acid in ACN; flow rate 1 mL/min; column = Phenomenex, Gemini NX C18 30 mm × 2.1 mm, 3 μm particle size; temperature 50 °C. <sup>b</sup> HPLC method B: solvent gradient 90% A @ 0 min, 10% A @ 3.5 min, 10% A @ 5 min; solvent A = 0.1% NH<sub>4</sub>OH in water; solvent B = 0.1% NH<sub>4</sub>OH in ACN; flow rate 1 mL/min; column = Waters Xterra C18, 30 mm × 2.1 mm, 3.5 μm particle size; temperature 50 °C.

**5-(3,4-Dimethoxyphenyl)-4-(1*H*-indol-5-ylamino)-3-pyridinecarbonitrile (**4p**).** A mixture of 4-chloro-5-(3,4-dimethoxyphenyl)-3-pyridinecarbonitrile (824 mg, 3 mmol), 5-aminoindole (396 mg, 3 mmol), and pyridine hydrochloride (345 mg, 3 mmol) in 2-ethoxyethanol (25 mL) was heated at reflux for 8 h, cooled to room temperature, and concentrated. The residue was purified by flash silica gel column chromatography eluting with 0–25% MeOH in dichloromethane to give 977 mg (88% yield) as a yellow-brown oil, which was triturated with MeOH/ethyl ether to give 525 mg (47%) of 5-(3,4-dimethoxyphenyl)-4-(1*H*-indol-5-ylamino)-3-pyridinecarbonitrile as a yellow-brown solid; mp: 170 °C (decompose). <sup>1</sup>H NMR (400 MHz, DMSO-*d*<sub>6</sub>) δ 11.19 (b, 1H), 8.96 (b, 1H), 8.60 (s, 1H), 8.22 (s, 1H), 7.41 (d, *J* = 1.5 Hz, 1H), 7.38–7.34 (m, 2H), 7.10–7.03 (m, 3H), 6.96 (dd, *J* = 8.2, 2.1 Hz, 1H), 6.41 (t, *J* = 2.1 Hz, 1H), 3.78 (s, 3H), 3.77 (s, 3H). See Table 3 for HPLC purity and HRMS data.

**4-Aryl-5-(3,4-Dimethoxyphenyl)-nicotinonitrile (**4a–r**).** Using the appropriate aniline analogues, **4a–r** were prepared following the procedure described for **4p**. Compounds were purified by RP-HPLC.

**Enzyme Kinetics Assays.** Adenosine 5'-triphosphate disodium salt hydrate (ATP), adenosine 5'-(3-trithriphosphate) tetralithium salt (ATPγS), synthetic polymer of sucrose (Ficoll-400), sucrose, adenosine diphosphate sodium salt (ADP), phosphoenolpyruvate (PEP), NADH, pyruvate kinase (PK), lactate dehydrogenase (LDH), adenosine 5'-(β,γ-imido)triphosphate tetralithium salt (AMPPNP), acetonitrile, DL-dithiothreitol (DTT), and the buffer HEPES were purchased from Sigma Chemical Co. (St. Louis, MO). Peptide substrates, inhibitors, and phosphorylated substrate peptides were from AnaSpec (San Jose, CA), SynPep (Dublin, CA), or Open Biosystems (Huntsville, AL). The enzymatic activity was determined at 25 °C using the coupled PK/LDH assay, at 340 nm on a Molecular Devices plate reader. The standard reaction, except where indicated, was carried out in a final volume of 80 μL, in 25 mM HEPES (pH 7.5), 10 mM MgCl<sub>2</sub>, 2 mM DTT, 0.008% Triton X-100, 100 mM NaCl, 20 units of PK, 30 units of LDH, 0.25 mM NADH, 2 mM PEP, and the PKCθ KD (0.156–0.312 μg/mL). *K*<sub>i</sub> values calculated according to the formula  $v = V_{\max}/(1 + (K_m/S)(1 + I/K_i))$ .

**FP Competition Displacement.** FP competition displacement experiment was measured on a Molecular Devices Analyst AD instrument. The 20 μL reactions were carried out in a 96-well black LJL low-volume plate in a buffer of 20 mM MOPS (Sigma), pH 7.0, 10 mM MgCl<sub>2</sub>, 0.005% Brij-35 (Sigma), 1.4 mM β-mercaptoethanol. The competition displacement reaction mixture contained 50 nM fluorescent probe, 125 nM PKCθ, and various concentrations of the inhibitor. The fluorescent probe *N*-(3',6'-dihydroxy-3-oxo-3*H*-spiro[2-benzofuran-1,9'-xanthen]-5-yl)-*N'*-(2-[3-[4-(1*H*-indol-3-yl)-2,5-dioxo-2,5-dihydro-1*H*-pyrrol-3-yl]-1*H*-indol-1-yl]ethyl)thiourea (FITC-

BIM-I) was prepared by coupling fluorescein isothiocyanate (FITC) with 3-[1-(2-aminoethyl)-1*H*-indol-3-yl]-4-(1*H*-indol-3-yl)-1*H*-pyrrole-2,5-dione. A control reaction mixture contained 50 nM fluorescent probe and various concentrations of the inhibitor. The reactions were incubated for 5–30 min at room temperature before measurement.

**NMR Binding.** The STD experiment<sup>34</sup> was performed on a 600 MHz Bruker Avance equipped with a cryoprobe at 25 °C, in 20 mM HEPES, pH = 7.5, 5 mM MgCl<sub>2</sub>, 5 mM DL-dithiothreitol (DTT), 100 mM NaCl, and 5% DMSO prepared in D<sub>2</sub>O. A 50 ms Gaussian pulse was used for selective excitation at the on and off resonance frequencies of the 0.7 ppm and -4 ppm, respectively, with a 1 ms delay in between the pulses for a 2 s excitation time. A presaturation pulse was used to minimize the residual water signal.

**PKCθ IMAP Kinase Assay.** All IC<sub>50</sub>s were measured by employing a modified IMAP protocol from Molecular Devices. The reaction buffer (R7209), detection reagent (R7284), and binding buffer (R7282), as well as the peptide substrate 5-FAM-RFARKGSL-RQKNV-OH (RP7032), were purchased from Molecular Devices. The kinase reaction was carried out in a final volume of 20 μL reaction buffer in a Corning Costar 384 well plate (Corning Costar 3710) containing compound, 1.0 nM full length human PKCθ (Panvera P2996), Three mM DL-dithiothreitol (DTT), 6 μM ATP, 100 nM of peptide, and 5% DMSO with an incubation time of 30 min. Then 50 μL detection reagents in binding buffer with dilution ratio of 1:800 was added to the reaction mixture and the fluorescence polarization was measured on an Envision 2100 (PerkinElmer Life Sciences).

**PKC Isoform IMAP Kinase Assay.** The same protocol as for PKCθ was also used in measuring compound IC<sub>50</sub>s for PKC isoforms including, PKCβ, PKCδ, PKCε, PKCη, and PKCζ (Panvera) using modified enzyme concentrations and incubation times.

**T Cell IL2 Production Assay.** T cells were enriched from spleens of 8–12 week old female PKCθ knockout mice or wild-type C57BL/6 mice (Taconic, Germantown, NY), using T cell enrichment columns (R&D Systems, Minneapolis, MN). The cells were resuspended in RPMI-1640 medium (Sigma) containing 10% fetal calf serum (FCS), penicillin/streptomycin, glutamine, nonessential amino acids, HEPES, sodium pyruvate, and BME vitamin solution (Sigma), and plated at 2 × 10<sup>6</sup>/mL in 96-well flat-bottomed plates coated with 20 mg/mL anti-CD3 and 4 mg/mL anti-CD28 (R&D Systems Inc., Minneapolis, MN), with a titration of the indicated compound or DMSO control. After 20–24 h incubation at 37 °C in 5% CO<sub>2</sub>, supernatants were harvested and IL-2 concentration was determined by ELISA (Invitrogen, Carlsbad, CA). The limit of assay sensitivity was 3.9 pg/mL.

**Molecular Modeling.** The X-ray structure of a compound with the 4-arylamino-3-pyridinecarbonitrile scaffold bound to phosphoinositide-dependent kinase-1 (PDK1) was obtained through soaking experiments (unpublished data). Backbone protein atoms from this

PDK1 structure and a PKC $\theta$ -staurosporine costructure<sup>15</sup> were superimposed to determine the initial placement of the pyridinecarbonitrile scaffold in the PKC $\theta$  ATP-binding site. As such, the models of compounds bound to PKC $\theta$  that are discussed in this manuscript were generated based on manual building followed by gradual minimization using the program CHARMM<sup>36</sup> and the all-atom force field.<sup>37</sup> Figure 3 was created in Maestro (Schrodinger, Inc., New York, NY, 2007).

**Acknowledgment.** We thank James LaRocque and Mariya Gazumiyani for HTS assay, Xidong Feng for HRMS data, Karl Malakian, Laura Lin, Ron Kriz and Mark Stahl for PKC $\theta$  protein expression and purification.

**Supporting Information Available:** HPLC chromatographic data and NMR spectra for **4a**–**4r**. This material is available free of charge via the Internet at <http://pubs.acs.org>.

## References

- Newton, A. C. Protein kinase C: structural and spatial regulation by phosphorylation, cofactors, and macromolecular interactions. *Chem. Rev.* **2001**, *101*, 2353–2364.
- Miyamoto, A.; Nakayama, K.; Imaki, H.; Hirose, S.; Jiang, Y.; Abe, M.; Tsukiyama, T.; Nagahama, H.; Ohno, S.; Hatakeyama, S.; Nakayama, K. I. Increased proliferation of B cells and auto-immunity in mice lacking protein kinase C delta. *Nature* **2002**, *416*, 865–869.
- Hug, H.; Sarre, T. F. Protein kinase C isoenzymes: divergence in signal transduction. *Biochem. J.* **1993**, *291*, 329–343.
- Baier, G.; Telford, D.; Giampa, L.; Coggeshall, K. M.; Baier-Bitterlich, G.; Isakov, N.; Altman, A. Molecular cloning and characterization of PKC theta, a novel member of the protein kinase C (PKC) gene family expressed predominantly in hematopoietic cells. *J. Biol. Chem.* **1993**, *268*, 4997–5004.
- Pfeiffer, C.; Kofler, K.; Gruber, T.; Tabrizi, N. G.; Lutz, C.; Maly, K.; Leitges, M.; Baier, G. Protein kinase C theta affects Ca<sup>2+</sup> mobilization and NFAT cell activation in primary mouse T cells. *J. Exp. Med.* **2003**, *197*, 1525–1535.
- Berg-Brown, N. N.; Gronski, M. A.; Jones, R. G.; Elford, A. R.; Deenick, E. K.; Odermatt, B.; Littman, D. R.; Ohashi, P. S. PKCtheta signals activation versus tolerance in vivo. *J. Exp. Med.* **2004**, *199*, 743–752.
- Marsland, B. J.; Soos, T. J.; Spath, G.; Littman, D. R.; Kopf, M. Protein kinase C theta is critical for the development of in vivo T helper (Th)2 cell but not Th1 cell responses. *J. Exp. Med.* **2004**, *200*, 181–189.
- Salek-Ardakani, S.; So, T.; Halteman, B. S.; Altman, A.; Croft, M. Differential regulation of Th2 and Th1 lung inflammatory responses by protein kinase C theta. *J. Immunol.* **2004**, *173*, 6440–6447.
- Salek-Ardakani, S.; So, T.; Halteman, B. S.; Altman, A.; Croft, M. Protein kinase C theta controls Th1 cells in experimental autoimmune encephalomyelitis. *J. Immunol.* **2005**, *175*, 7635–7641.
- Tan, S. L.; Zhao, J.; Bi, C.; Chen, X. C.; Hepburn, D. L.; Wang, J.; Sedgwick, J. D.; Chintalacheruvu, S. R.; Na, S. Resistance to experimental autoimmune encephalomyelitis and impaired IL-17 production in protein kinase C theta-deficient mice. *J. Immunol.* **2006**, *176*, 2872–2879.
- Giannoni, F.; Lyon, A. B.; Wareing, M. D.; Dias, P. B.; Sarawar, S. R. Protein kinase C theta is not essential for T-cell-mediated clearance of murine gammaherpesvirus 68. *J. Virol.* **2005**, *79*, 6808–6813.
- Healy, A. M.; Izmailova, E.; Fitzgerald, M.; Walker, R.; Hattersley, M.; Silva, M.; Siebert, E.; Terkelsen, J.; Picarella, D.; Pickard, M. D.; LeClair, B.; Chandra, S.; Jaffee, B. PKC-theta-deficient mice are protected from Th1-dependent antigen-induced arthritis. *J. Immunol.* **2006**, *177*, 1886–1893.
- Chaudhary, D.; Kasaian, M. PKCtheta: A potential therapeutic target for T-cell-mediated diseases. *Curr. Opin. Investig. Drugs* **2006**, *7*, 432–437.
- Czerwinski, R.; Aulabaugh, A.; Greco, R. M.; Olland, S.; Malakian, K.; Wolfrom, S.; Lin, L.; Kriz, R.; Stahl, M.; Huang, Y.; Liu, L.; Chaudhary, D. Characterization of protein kinase C theta activation loop autophosphorylation and the kinase domain catalytic mechanism. *Biochemistry* **2005**, *44*, 9563–9573.
- Xu, Z. B.; Chaudhary, D.; Olland, S.; Wolfrom, S.; Czerwinski, R.; Malakian, K.; Lin, L.; Stahl, M. L.; Joseph-McCarthy, D.; Benander, C.; Fitz, L.; Greco, R.; Somers, W. S.; Mosyak, L. Catalytic domain crystal structure of protein kinase C-theta (PKCtheta). *J. Biol. Chem.* **2004**, *279*, 50401–50409.
- Mecklenbrauer, I.; Saijo, K.; Zheng, N. Y.; Leitges, M.; Tarakhovskiy, A. Protein kinase C delta controls self-antigen-induced B-cell tolerance. *Nature* **2002**, *416*, 860–865.
- Yaney, G. C.; Fairbanks, J. M.; Deeney, J. T.; Korchak, H. M.; Tornheim, K.; Corkey, B. E. Potentiation of insulin secretion by phorbol esters is mediated by PKC- $\alpha$  and nPKC isoforms. *Am. J. Physiol.* **2002**, *283*, E880–E888.
- Kotsonis, P.; Funk, L.; Proutzos, C.; Iannazzo, L.; Majewski, H. Differential abilities of phorbol esters in inducing protein kinase C (PKC) down-regulation in noradrenergic neurones. *Br. J. Pharmacol.* **2001**, *132*, 489–499.
- Lee, H.-W.; Smith, L.; Pettit, G. R.; Smith, J. B. Bryostatin 1 and phorbol ester down-modulate protein kinase C- $\alpha$  and - $\epsilon$  via the ubiquitin/proteasome pathway in human fibroblasts. *Mol. Pharmacol.* **1997**, *51*, 439–447.
- Kortmansky, J.; Schwartz, G. K. Bryostatin-1: A Novel PKC Inhibitor in Clinical Development. *Cancer Invest.* **2003**, *21*, 924–936.
- Irie, K.; Ohigashi, H. Synthesis and functional analysis of the cysteine-rich domains of protein kinase C (PKC) for development of new medicinal leads with PKC isozyme and C1 domain selectivity. *Yuki Gosei Kagaku Kyokaiishi* **2002**, *60*, 563–572.
- Choi, Y.; Pu, Y.; Peach, M. L.; Kang, J. H.; Lewin, N. E.; Sigano, D. M.; Garfield, S. H.; Blumberg, P. M.; Marquez, V. E. Conformationally constrained analogues of diacylglycerol (DAG). 28. DAG-dioxolanones reveal a new additional interaction site in the C1b domain of PKC delta. *J. Med. Chem.* **2007**, *50*, 3465–3481.
- Goekjian, P. G.; Jirousek, M. R. Protein kinase C inhibitors as novel anticancer drugs. *Expert Opin. Investig. Drugs* **2001**, *10*, 2117–2140.
- Fabbro, D.; Ruetz, S.; Bodis, S.; Pruschy, M.; Csermak, K.; Man, A.; Campochario, P.; Wood, J.; O'Reilly, T.; Meyer, T. PKC412: a protein kinase inhibitor with a broad therapeutic potential. *Anti-Cancer Drug Des.* **2000**, *15*, 17–28.
- Mizuno, K.; Noda, K.; Ueda, Y.; Hanaki, H.; Saido, T. C.; Ikuta, T.; Kuroki, T.; Tamaoki, T.; Hirai, S.; Osada, S.; et al. UCN-01, an anti-tumor drug, is a selective inhibitor of the conventional PKC subfamily. *FEBS Lett.* **1995**, *359*, 259–261.
- Mizuno, K.; Saido, T. C.; Ohno, S.; Tamaoki, T.; Suzuki, K. Staurosporine-related compounds, K252a and UCN-01, inhibit both cPKC and nPKC. *FEBS Lett.* **1993**, *330*, 114–6.
- McGill, J. B.; King, G. L.; Berg, P. H.; Price, K. L.; Kles, K. A.; Bastyr, E. J.; Hyslop, D. L. Clinical safety of the selective PKC-beta inhibitor, ruboxistaurin. *Expert Opin. Drug Saf.* **2006**, *5*, 835–845.
- Jirousek, M. R.; Gillig, J. R.; Gonzalez, C. M.; Heath, W. F.; McDonald, J. H.; Neel, D. A.; Rito, C. J.; Singh, U.; Stramm, L. E.; Melikian-Badalian, A.; Baevsky, M.; Ballas, L. M.; Hall, S. E.; Winneroski, L. L.; Faul, M. M. (S)-13-[(Dimethylamino)methyl]-10,11,14,15-tetrahydro-4,9:16,21-dimetheno-1H,13H-dibenzo[e,k]pyrrolo[3,4-h][1,4,13]oxadiazacyclohexadecene-1,3(2H)-dione (LY33531) and Related Analogs: Isoenzyme Selective Inhibitors of Protein Kinase C $\beta$ . *J. Med. Chem.* **1996**, *39*, 2664–2671.
- Mackay, H. J.; Twelves, C. J. Targeting the protein kinase C family: are we there yet? *Nat. Rev. Cancer* **2007**, *7*, 554–562.
- Cywin, C. L.; Dahmann, G.; Prokopowicz, A. S.; Young, E. R. R.; Magolda, R. L.; Cardozo, M. G.; Cogan, D. A.; DiSalvo, D.; Ginn, J. D.; Kashem, M. A.; Wolak, J. P.; Homon, C. A.; Farrell, T. M.; Grbic, H.; Hu, H.; Kaplita, P. V.; Liu, L. H.; Spero, D. M.; Jeanfavre, D. D.; O'Shea, K. M.; White, D. M.; Woska, J. R.; Brown, M. L. Discovery of potent and selective PKC $\theta$  inhibitors. *Bioorg. Med. Chem. Lett.* **2007**, *17*, 225–230.
- Caliper Life Sciences.
- Huang, X. Equilibrium competition binding assay: inhibition mechanism from a single dose response. *J. Theor. Biol.* **2003**, *225*, 369–376.
- Bisindolylmaleimide I. 2-[1-(3-Dimethylaminopropyl)-1H-indol-3-yl]-3-(1H-indol-3-yl)-maleimide.
- Mayer, M.; Meyer, B. Characterization of ligand binding by saturation transfer difference NMR spectroscopy. *Angew. Chem., Int. Ed.* **1999**, *38*, 1784–1788.
- Molecular Devices. <http://www.moleculardevices.com/pages/reagents/imapintro.html>.
- Brooks, B. R.; Bruccoleri, R. E.; Olafson, B. D.; States, D. J.; Swaminathan, S.; Karplus, M. CHARMM: a program for macromolecular energy, minimization, and dynamics calculations. *J. Comput. Chem.* **1983**, *4*, 187–217.
- MacKerell, A. D., Jr.; Bashford, D.; Bellott, M.; Dunbrack, R. L.; Evanseck, J. D.; Field, M. J.; Fischer, S.; Gao, J.; Guo, H.; Ha, S.; Joseph-McCarthy, D.; Kuchnir, L.; Kuczera, K.; Lau, F. T. K.; Mattos, C.; Michnick, S.; Ngo, T.; Nguyen, D. T.; Prodhom, B.; Reiher, W. E., III; Roux, B.; Schlenkrich, M.; Smith, J. C.; Stote, R.; Straub, J.; Watanabe, M.; Wiorkiewicz-Kuczera, J.; Yin, D.; Karplus, M. All-Atom Empirical Potential for Molecular Modeling and Dynamics Studies of Proteins. *J. Phys. Chem. B* **1998**, *102*, 3586–3616.